JACS
JOURNAL OF THE AMERICAN CHEMICAL SOCIETY

Communication

pubs.acs.org/JACS

Plasmonic Imaging of Electrochemical Oxidation of Single Nanoparticles

Yimin Fang,[†] Wei Wang,*[,†] Xiang Wo,[†] Yashuang Luo,[†] Shaowei Yin,[†] Yixian Wang,[‡] Xiaonan Shan,[‡] and Nongjian Tao*[,†,‡]

[†]State Key Laboratory of Analytical Chemistry for Life Science, School of Chemistry and Chemical Engineering, Nanjing University, Nanjing 210093, China

[‡]Center for Bioelectronics and Biosensors, Biodesign Institute, Arizona State University, Tempe, Arizona 85287, United States

Supporting Information

ABSTRACT: Measuring electrochemical activities of nanomaterials is critical for creating novel catalysts, for developing ultrasensitive sensors, and for understanding fundamental nanoelectrochemistry. However, traditional electrochemical methods measure a large number of nanoparticles, which wash out the properties of individual nanoparticles. We report here a study of transient electrochemical oxidation of single Ag nanoparticles during collision with an electrode and voltammetry of single nanoparticles immobilized on the electrode using a plasmonic-based electrochemical current microscopy. This technique images both electrochemical reaction and size of the same individual nanoparticle, enabling quantitative examination of size-dependent electrochemical activities at single nanoparticle level. The imaging capability further allows detection of the reaction kinetics of each individual nanoparticle and analysis of the average behaviors of multiple nanoparticles. The average kinetics and size dependence can be accurately described by the Tafel equation, but there is a large variability between different nanoparticles, which underscores the importance of single nanoparticle analysis.

Nanoscale materials are interesting because of their unique properties and broad applications.[1] An important example is the electrochemical properties of nanoparticles,[2−4] which have found applications in catalysts[5] and chemical sensors.[6] Evidence has shown that the electrochemical properties of each nanoparticle is different, depending on its size,[7,8] shape,[9,10] composition, and surface states.[11,12] However, traditional electrochemical methods measure a large number of nanoparticles, which wash out the properties of individual nanoparticles. A technique for studying single nanoparticle electrochemistry is thus needed in order to understand the relationship between the structure and function of nanoparticles.[9,13,14] It has been reported recently that electrochemical reactions of single nanoparticles can be studied by detecting the transient electrochemical current as individual nanoparticles collide with a microelectrode.[15−18] Because this method detects transient events, it cannot measure the current of single nanoparticles as the potential is varied (voltammetry). Moreover, it cannot identify which nanoparticle is responsible for a transient current, which is required to study the relationship between size and reactivity of a nanoparticle.[9,13]

Here we report a study of electrochemical oxidation of single Ag nanoparticles with plasmonic-based electrochemical current microscopy (P-ECM), a technique that images both electrochemical reaction and size of the nanoparticles. We detect transient electrochemical oxidation during the collision of individual nanoparticles with the electrode, perform voltammetry on single nanoparticles immobilized on the electrode, examine size-dependent electrochemical oxidation of the nanoparticles, and model the observed oxidation kinetics with the Butler−Volmer formalism.

The principle of P-ECM in the present work is to detect electrochemical reaction-induced change in the Ag nanoparticle size with plasmonic imaging, which is different from our previous report[19,20] that detected local concentration of a reactant or product. Figure 1A shows the experimental setup and principle of

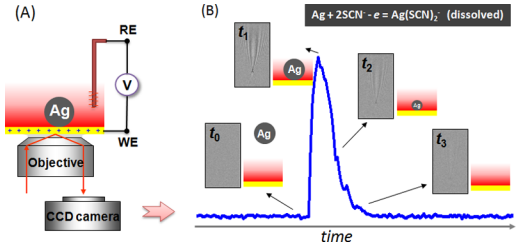

Figure 1. (A) Schematic illustration of P-ECM imaging of single nanoparticle electrochemistry, gold chip as working electrode (WE), and Ag/AgCl as reference electrode (RE). (B) Transient collision and electrochemical oxidation of a single Ag nanoparticle correlated with the transient plasmonic image intensity (blue curve).

P-ECM. Light from a superluminescent light emitting diode is directed onto an Au electrode at an appropriate incident angle via an optical microscope objective to excite surface plasmons and the reflected light is collected with the same objective to form a surface plasmon resonance (SPR) image.

P-ECM was carried out by either holding the electrode potential at a fixed value or sweeping it linearly over a range. When the potential was held above the oxidation potential, random collisions of the individual Ag nanoparticles with the

Received: July 14, 2014
Published: August 20, 2014

   dx.doi.org/10.1021/ja507097y | J. Am. Chem. Soc. 2014, 136, 12584−12587

electrode resulted in the oxidation of the nanoparticles (Figure 1B). Note that the parabolic tail in the image of each nanoparticle was due to the scattering of the surface plasmon wave by the nanoparticle located within the range of the evanescent wave (~200 nm depth, red box in Figure 1A).[21] The image intensity decreased over time during the electrochemical process. This was because the oxidized Ag was soluble in the electrolyte containing SCN^- ion ($Ag + 2SCN^- - e = Ag(SCN)_2^-$), and the Ag nanoparticles decreased in size during oxidation. As we will show later, the decreasing image intensity was directly related to the electrochemical oxidation current. By converting the image intensity into current, P-ECM allowed imaging of local electrochemical current of multiple single nanoparticles simultaneously.

Figure 2A–E show several snapshots of the collision and oxidation of 3 Ag nanoparticles on the electrode at −50 mV (vs Ag/AgCl). A movie of the entire process is provided in Movie S1 in the Supporting Information (SI). Before the collision of the nanoparticles with the electrode, the electrode surface was clean (Figure 2A). 0.22 s after starting recording the movie, three Ag nanoparticles, marked by 1, 2 and 3, hit the electrode surface simultaneously (Figure 2B). Note that simultaneous collision of multiple nanoparticles cannot be separated with the traditional electrochemical detection because the transient currents from different nanoparticles overlap in time domain, which underscores the value of spatial resolution offered by P-ECM in the present work. As these nanoparticles were oxidized and dissolved, they shrank and eventually completely disappeared from the surface. The time duration to completely dissolve varied from nanoparticle to nanoparticle, indicating different oxidation rates for different nanoparticles. For example, nanoparticle 1 dissolved first (Figure 2C), then nanoparticle 2 (Figure 2D), and followed by nanoparticle 3 (Figure 2E).

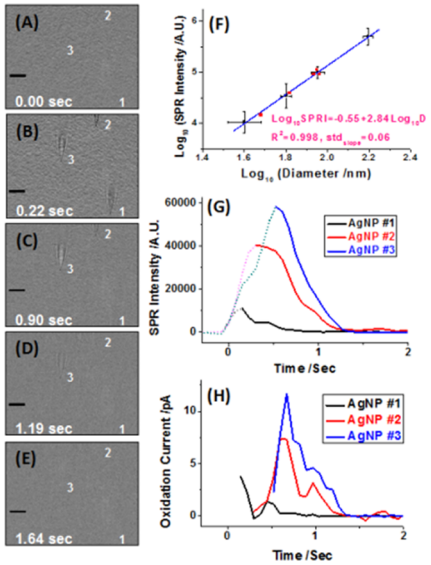

Figure 2. (A–E) Snapshots of plasmonic images of three individual Ag nanoparticles during a typical collision-oxidation process. Scale bars (black), 10 μm. (F) Plasmonic image intensity vs nanoparticle size by DLS (black dots) and AFM (red dots). (G) Transient plasmonic image intensity curves of the three individual Ag nanoparticles shown in (A–E). (H) Transient electrochemical current of the Ag nanoparticles obtained from the plasmonic image intensity.

To confirm that the image intensity decrease was indeed due to the electrochemical oxidation of Ag, we performed the experiment at different electrode potentials, and observed intensity decrease only when the potential was above the redox potential of Ag nanoparticles. Despite of the variability among different nanoparticles, the overall trend was that the higher the electrode potential, the faster was the oxidation. This behavior is clearly shown in Movie S2 in the SI. Below the redox potential, the images of Ag nanoparticles did not change over time (Movie S3, SI). Note SCN^- is required for the complete dissolution (disappearance) of the Ag nanoparticles. In the absence of SCN^- in the electrolyte, the image intensity of Ag nanoparticles also decreased, but it did not disappear completely even when the electrode was held far above the oxidation potential (Movie S4 and Figure S1, SI). The change in the image intensity of the Ag nanoparticles in the absence of SCN^- was due to the conversion of Ag to insoluble Ag_2O nanoparticles, which caused a change in the optical property of the Ag/Ag_2O nanoparticles. These results demonstrated that the disappearance of nanoparticles was indeed due to the oxidation and dissolution, instead of detachment of Ag nanoparticles from the electrode surface.

The SPR image intensity of a Ag nanoparticle is expected to be proportional to its volume.[19] In order to confirm this, we measured the image intensities of Ag nanoparticles with different diameters. Figure 2F plots the image intensity in logarithmic scale vs nanoparticle diameter, which shows linear dependence with a slope of 2.84, close to 3. We attribute the small deviation to the decay (decay length of ~200 nm) of the evanescent wave associated with surface plasmons into the solution phase from the electrode surface. In other words, the nanoparticle on the electrode did not experience a uniform electric field in the direction normal to the electrode surface.

Figure 2G shows the transient SPR image intensity of 3 nanoparticles during the collision with the electrode, showing an increase (dashed line) followed by a decrease (solid line). The increase occurred because the nanoparticle approached the electrode surface, and the decrease was due to the electrochemical oxidation of the nanoparticle. Using the calibration curve shown in Figure 2F, we obtained the volume (diameter) of each nanoparticle from the SPR image intensity. Because the change in the volume is proportional to the amount of charge transfer associated with the electrochemical oxidation of Ag, we determined transient electrochemical oxidation current of each nanoparticle from the decrease of the image intensity as shown in Figure 2H. The transient current curves measured with P-ECM are similar to those obtained with ultramicroelectrode,[15−18] but the P-ECM approach allows simultaneously detection of collision of multiple nanoparticles and the study of size dependence of the electrochemical oxidation.

The kinetics of the electrochemical oxidation of a nanoparticle and its dependence on the nanoparticle size can be described with the Tafel equation given by:

$$i(t) = 4\pi r^2(t)\cdot nF\cdot k_0\cdot e^{\alpha\frac{nF}{RT}(E-E_0)} \quad (1)$$

where $i(t)$ and $r(t)$ are the transient current and radius of the nanoparticle, n is the number of electron transfer per atom, F is the Faraday constant, k_0 is the electron transfer rate constant, α is the charge transfer coefficient, R is the gas constant, T is temperature, E is the applied potential, and E_0 is the formal potential, respectively. According to eq 1, and also the fact that the amount of charge transfer is equal to the number of dissolved (oxidized) Ag atoms from the particles,[20] we have (see SI):

dx.doi.org/10.1021/ja507097y | J. Am. Chem. Soc. 2014, 136, 12584−12587

$$r(t) = r_0 - \frac{m_{Ag}N_A}{\rho}k_0 e^{\alpha\frac{nF}{RT}(E-E_0)}t \quad (2)$$

where ρ, m_{Ag}, N_A, and r_0 are density of silver, mass of silver atom, Avogadro's constant, and the original radius of the particle, respectively. Eq 2 describes how the size of a nanoparticle depends on time and potential. Note that the current model assumes isotropic oxidation and dissolution of nanoparticles, which fits the experimental data well for the spherical nanoparticles studied in this work (see below). The effect of crystal facets with different reactivity, especially in highly anisotropic nanostructures (e.g., rods), will be studied in a more accurate way in future work.

In order to examine the oxidation kinetics predicted by the above model, we performed the electrochemical oxidation experiment at different electrode potentials, ranging from −75 to 100 mV (vs Ag/AgCl). Transient SPR image intensity curves averaged over 50 individual nanoparticles at different electrode potentials are shown in Figure 3A. The result shows that the

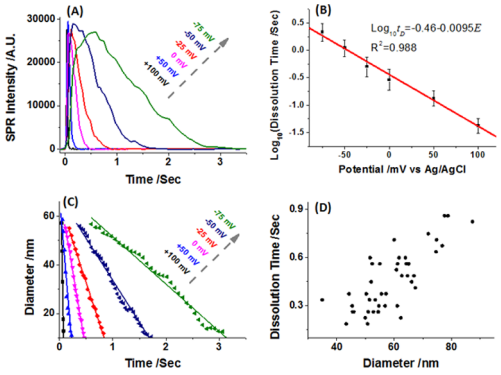

Figure 3. Kinetics of electrochemical oxidation of single Ag nanoparticles. (A) Average transient plasmonic image intensity of Ag nanoparticles at different electrode potentials (averaged over 50 nanoparticles). (B) Average dissolution time in logarithmic scale vs electrode potential. (C) Average diameter of the Ag nanoparticles vs time during dissolution. (D) Dissolution times of different nanoparticles vs their diameters at −25 mV.

nanoparticles dissolved much faster at higher electrode potentials, which can be understood quantitatively based on the above model. According to eq 2, the average dissolution time (t_D) is given by:

$$t_D = \frac{r_0\rho}{m_{Ag}N_A k_0 e^{\alpha\frac{nF}{RT}(E-E_0)}} \quad (3)$$

so that the dissolution time in logarithmic scale decreases proportionally to the overpotential. This prediction is in excellent agreement with the experimental data shown in Figure 3B. From the slope of the plot in Figure 3B, the charge transfer coefficient α was determined to be 0.59, which is in its normal range from 0.3 to 0.7.[22]

Another prediction of the kinetic model is that the average size (radius) of the nanoparticles decreases linearly with time during the dissolution process, as described by eq 2. We determined the transient size of each nanoparticle from the SPR image intensity during the electrochemical oxidation using the calibration curve in Figure 2F. The results as plotted in Figure 3C indeed show that the average diameter of nanoparticles decreases linearly with time at all electrode potentials. The slope of the linear relationship, however, depends on the electrode potential, which is also consistent with the kinetic model (see Figure S6, SI).

The average size and dissolution time are in excellent agreement with the kinetic model based on the Tafel equation as discussed above. Because P-ECM allows the study of each individual nanoparticles, we also studied the kinetics of individual nanoparticles. Figure 3D plots the distribution of dissolution time of 43 Ag nanoparticles of different sizes at −25 mV. The average dissolution time is approximately proportional to the nanoparticle diameter, however there is a large variation in the dissolution time for a given size of the nanoparticles, which underscores the importance of studying electrochemical oxidation of each nanoparticle. We will return to this later.

In addition to studying the transient electrochemical oxidation of individual nanoparticles, we performed linear sweep voltammetry of single nanoparticles. For this study, Ag nanoparticles were first immobilized on the electrode prior to the electrochemical oxidation. Subsequently, the electrode potential was swept linearly from −300 to +200 mV at a rate of 20 mV/s. A movie of the entire process is provided in Movie S5, SI, and Figure 4 presents a few snapshots during the potential

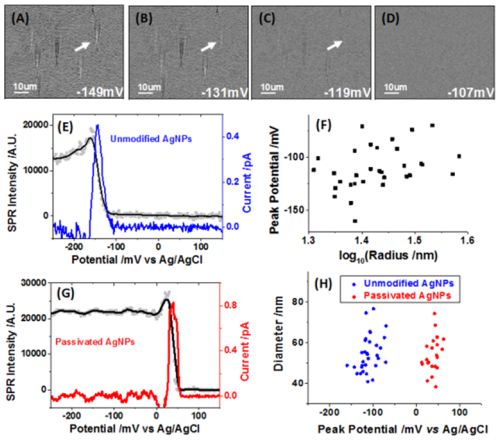

Figure 4. Voltammetry of single nanoparticles. (A–D) Snapshots of the dissolution processes of multiple Ag nanoparticles during a potential cycle. (E) Plasmonic image intensity (black curve) and corresponding electrochemical current (blue) of a single unmodified Ag nanoparticle vs potential. (F) Peak potential of single Ag nanoparticle exhibits weak correlation with the size of single nanoparticle. (G) Plasmonic intensity (black) and corresponding electrochemical current (red) of a single passivated Ag nanoparticle vs potential. (H) Correlation between oxidation peak potentials and diameters of different Ag nanoparticles. Blue dots: unmodified, and red dots: passivated Ag nanoparticles.

sweep. The image intensity of each nanoparticle decreases with the increasing electrode potential, and eventually disappears. The SPR image intensity for one of the nanoparticles is plotted vs the electrode potential in Figure 4E (black curve). The corresponding voltammogram is also shown in Figure 4E (blue curve), which reveals a pronounced oxidation peak in the electrochemical current at ∼ −140 mV.

Different nanoparticles show similar voltammograms, but the oxidation peaks occur at different potentials for different nanoparticles. Figure 4F plots the oxidation peak potentials of 37 nanoparticles with diameters varying from 35 to 80 nm, which shows that on average the peak potential increases with the diameter of the nanoparticle. This size dependence can be understood based on the kinetic model described by eqs 1 and 2.

dx.doi.org/10.1021/ja507097y | J. Am. Chem. Soc. 2014, 136, 12584−12587

As shown in the SI, the peak potential (E_p) based on the kinetic model is related to the nanoparticle radius (r_0) according to

$$E_p = E_0 + \frac{2.303RT}{\alpha nF}\log_{10}\left(\frac{r_0 v \alpha n F \rho}{3RTm_{Ag}N_A k_0}\right) \quad (4)$$

where v is potential sweep rate. The experimental data can be fit with eq 4, with $\alpha = 0.65$ (red curve, Figure 4F). This α value is in good agreement with the result from collision experiments under constant potential, further validating the proposed oxidation-induced dissolution model.

The average behaviors of the nanoparticles can be described with the kinetic model described above, but the variation of the oxidation peak potentials of the individual nanoparticles can be as large as 50 mV. We believe that this variation is at least partially due to the surface chemistry of the individual nanoparticles. In order to confirm this hypothesis, we modified Ag nanoparticles with cysteine, which provides a passivation layer to the nanoparticles. The image intensity profile (black curve) and the voltammogram (red curve) of a passivated nanoparticle are shown in Figure 4G (see Movie S6, SI). Compared with unpassivated nanoparticles, the oxidation peak potential shifts to a higher value by as much as 150 mV. A more detailed comparison of the oxidation peak potentials for cysteine-modified and unmodified nanoparticles is given in Figure 4H, which shows that the oxidation peak potentials of the former are systematically higher than the latter.

The surface passivation may affect the electrochemical oxidation by increasing the contact resistance between a nanoparticle and the electrode surface. Based on the single molecule conductance values measured by us with a break junction method[23] and the peak current measured here, the estimated upper limit in the potential drop across the nanoparticle-electrode interface is ~0.1 mV, which is insignificant compared to the observed variation in the oxidation potential. This consideration rules out the contact resistance as the mechanism for the observed peak potential variation. Another possible mechanism is the passivation of the nanoparticle surface with cysteine, which prevents rapid oxidation of surface Ag atoms on the nanoparticle. We believe that impurity or contaminant molecules on the surface of the nanoparticles will shift the oxidation peak potential to a higher value.

We demonstrated a study of single nanoparticle electrochemistry using P-ECM. The spatial resolution of P-ECM allowed us to resolve the electrochemical currents from simultaneous collisions of multiple nanoparticles with an electrode, study the oxidation kinetics of each individual nanoparticle, and analyze the average oxidation kinetics of many nanoparticles. It also allowed us to obtain precise size information on the individual nanoparticles from the SPR image intensity, making it possible to examine size-dependent electrochemical activities of single nanoparticles. In addition to measuring transient current, we performed voltammetry of single nanoparticles immobilized on the electrode and extracted the oxidation peak potentials of individual nanoparticles. The average electrochemical oxidation kinetics and its dependence on the nanoparticle size could be quantitatively described with the Tafel equation, but there was a large nanoparticle to nanoparticle variation for a given size, which was attributed to the variation in the surface chemistry of different nanoparticles. We believe that the P-ECM capabilities demonstrated here can be applied to study basic electrochemical processes and develop electrochemical applications of nanoscale materials.

■ ASSOCIATED CONTENT

Supporting Information

Experimental details, data analysis, characterization of Ag nanoparticles, descriptions of movies. This material is available free of charge via the Internet at http://pubs.acs.org.

■ AUTHOR INFORMATION

Corresponding Authors

wei.wang@nju.edu.cn
njtao@asu.edu

Notes

The authors declare no competing financial interest.

■ ACKNOWLEDGMENTS

We thank the financial support from National Natural Science Foundation of China (NSFC, grant no. 21327008), 1000 young talent program, and Multidisciplinary University Research Initiative (MURI, FA9550-14-1-0003).

■ REFERENCES

(1) Zach, M. P.; Ng, K. H.; Penner, R. M. *Science* **2000**, *290*, 2120.
(2) Chen, S.; Ingram, R. S.; Hostetler, M. J.; Pietron, J. J.; Murray, R. W.; Schaaff, T. G.; Khoury, J. T.; Alvarez, M. M.; Whetten, R. L. *Science* **1998**, *280*, 2098.
(3) Tian, N.; Zhou, Z. Y.; Sun, S. G.; Ding, Y.; Wang, Z. L. *Science* **2007**, *316*, 732.
(4) Oja, S. M.; Wood, M.; Zhang, B. *Anal. Chem.* **2013**, *85*, 473.
(5) Wu, B. H.; Zheng, N. F. *Nano Today* **2013**, *8*, 168.
(6) Chen, A. C.; Chatterjee, S. *Chem. Soc. Rev.* **2013**, *42*, 5425.
(7) Ivanova, O. S.; Zamborini, F. P. *J. Am. Chem. Soc.* **2010**, *132*, 70.
(8) Redmond, P. L.; Hallock, A. J.; Brus, L. E. *Nano Lett.* **2005**, *5*, 131.
(9) Lai, S. C. S.; Dudin, P. V.; Macpherson, J. V.; Unwin, P. R. *J. Am. Chem. Soc.* **2011**, *133*, 10744.
(10) Porter, N. S.; Wu, H.; Quan, Z. W.; Fang, J. Y. *Acc. Chem. Res.* **2013**, *46*, 1867.
(11) Suntivich, J.; Xu, Z. C.; Carlton, C. E.; Kim, J.; Han, B. H.; Lee, S. W.; Bonnet, N.; Marzari, N.; Allard, L. F.; Gasteiger, H. A.; Hamad-Schifferli, K.; Shao-Horn, Y. *J. Am. Chem. Soc.* **2013**, *135*, 7985.
(12) Tompsett, D. A.; Parker, S. C.; Islam, M. S. *J. Am. Chem. Soc.* **2014**, *136*, 1418.
(13) Kleijn, S. E. F.; Lai, S. C. S.; Miller, T. S.; Yanson, A. I.; Koper, M. T. M.; Unwin, P. R. *J. Am. Chem. Soc.* **2012**, *134*, 18558.
(14) Li, Y. X.; Cox, J. T.; Zhang, B. *J. Am. Chem. Soc.* **2010**, *132*, 3047.
(15) Xiao, X. Y.; Fan, F. R. F.; Zhou, J. P.; Bard, A. J. *J. Am. Chem. Soc.* **2008**, *130*, 16669.
(16) Xiao, X. Y.; Bard, A. J. *J. Am. Chem. Soc.* **2007**, *129*, 9610.
(17) Rees, N. V.; Zhou, Y. G.; Compton, R. G. *RSC Adv.* **2012**, *2*, 379.
(18) Zhou, Y. G.; Rees, N. V.; Compton, R. G. *Angew. Chem., Int. Ed.* **2011**, *50*, 4219.
(19) Wang, S. P.; Shan, X. N.; Patel, U.; Huang, X. P.; Lu, J.; Li, J. H.; Tao, N. J. *Proc. Natl. Acad. Sci. U.S.A.* **2010**, *107*, 16028.
(20) Hill, C. M.; Pan, S. L. A. *J. Am. Chem. Soc.* **2013**, *135*, 17250.
(21) Yu, H.; Shan, X. N.; Wang, S. P.; Chen, H. Y.; Tao, N. J. *ACS Nano* **2014**, *8*, 3427.
(22) Bard, A. J.; Faulkner, L. R. *Electrochemical Methods: Fundamentals and Application*, 2nd ed.; Wiley: Hoboken, NJ, 2000.
(23) Chen, F.; Li, X. L.; Hihath, J.; Huang, Z. F.; Tao, N. J. *J. Am. Chem. Soc.* **2006**, *128*, 15874.